AIAA Liquid Rocket Initiative

Grunt Engine Critical Design Review

Prepared by Ian Brown, Bartosz Wielgosz, Endika Llano, Calvin Berg, Shreya Bista, and Pedro Leite

March 2, 2022

Contents

Nomenclature

Symbols

α, β	spray angle curve fitting factors
ΔP	pressure drop
$\dot{m}$	mass flow rate
γ	heat capacity ratio
ρ	density
σ	Bartz correlation correction factor
A	area
a	thermal diffusivity $= \frac{k}{\rho C_v}$
A_{eff}	area enclosed by o-ring inner diameter
C_d	discharge coefficient
C_p	specific heat at constant pressure
d	diameter
F	thrust
F_{bolts}	total bolt clamping force
G	annular gap size
h	heat transfer coefficient
K	compressive response force between chamber and manifold plates
k	thermal conductivity
L^*	characteristic length
LMR	local momentum ratio
O	o-ring compressive force
P	pressure
Pr	Prandtl number of combustion gases
R	specific gas constant for combustion mixture
r_c	throat radius of curvature
T	temperature
T_i	initial wall temperature
U	injection velocity
V	volume
v_e	nozzle exit velocity
C^*	characteristic velocity

Subscripts

c	chamber
f	fuel
m	manifold
o	oxidizer
t	throat
w	wall

1 Introduction

The AIAA Liquid Rocket Initiative is a student group founded with the intent of providing students with hands-on experience with liquid rocket engine design and testing. The Grunt engine is our first attempt at liquid engine design. Grunt is a simple thrust chamber assembly which we will attach to the test stand at Purdue's Maurice J. Zucrow Laboratories to verify our injector concept, and to demonstrate our ability to build liquid rocket engines to our sponsors, as well as to the University of Illinois at Urbana-Champaign Department of Aerospace Engineering.

2 Design Overview

Grunt is an 1100 lbf Jet-A/LOx liquid rocket engine thrust chamber assembly. Our injector geometry is a single-element, oxidizer-centered pintle injector. Our combustion chamber will be a carbon steel billet with a conical nozzle geometry milled into it. The assembly will be bolted together with a flange setup.

2.1 Design Requirements

The primary objective of this project is to demonstrate that we can build an engine that produces thrust. However, to constrain our design process, and to avoid as best we can the need for large-scale design changes in future iterations, we have defined secondary requirements for the thrust and chamber pressure.

In order to choose a thrust objective, we thought about the future hypothetical use of the engine. We wanted to design an engine that we could improve over time, make it flight ready, and eventually implement on a rocket of a size that we could handle.

Initial sizing was performed using a simplified model of the dimensions and mass of a future rocket. This was done by treating the body of the rocket as a cylinder with a density equal to that of water.[1] With a diameter of 30 cm ($\approx$ 1 foot) and a height of 3 m ($\approx$ 10 feet), we get a mass of around 200 kg (440 lbm). For a thrust to weight ratio (at liftoff) of 2.5, we get a thrust of 5kN ($\approx$ 1100 lbf).

Mission Requirement: The engine shall produce thrust

Secondary Requirements:

1. The engine chamber pressure shall reach 20.7 bar (300 psi)
2. The engine shall produce 1100 lbf of thrust

2.2 Engine Sizing

We used CEARUN by NASA [3] to determine the conditions inside the combustion chamber, as well as the thrust coefficient and nozzle exhaust velocity, assuming an optimally expanded nozzle at sea level. A shifting equilibrium calculation was used to determine the properties of the combustion. The inputs into the CEA calculation were the propellants, the O/F ratio (determined based on past experience [5] [8]), the chamber pressure, and the nozzle exit pressure (1 atm).

A MATLAB script (Appendix A) was used to size the engine. The thrust chamber consists of a cylindrical combustion chamber with a conical nozzle. The volume of the combustion chamber is calculated with the characteristic length (L^*), a parameter that determines the propellant residence time in the chamber, and hence, the chamber efficiency. The characteristic length has been experimentally determined for several different propellant combinations, including kerosene/LOx [11].

$$V_c = L^* \cdot A_t \tag{1}$$

According the literature we consulted, the characteristic length for a kerosene/LOx combustion chamber should be between 1.02 and 1.27 m (3.35 to 4.17 ft) [11]. We chose to use a characteristic length of 0.9 m (2.95 ft) to make our design more manufacturable. This will reduce the residence time of the propellants in the combustion chamber, leading to a small efficiency loss due to combustion occurring in the nozzle exit.

The throat area was calculated using the ideal characteristic velocity equation, outlined in [7]:

$$C^* = \sqrt{\frac{1}{\gamma}\left(\frac{\gamma+1}{2}\right)^{\frac{\gamma+1}{\gamma-1}} RT_c} \tag{2}$$

Combining this with the definition of characteristic velocity, $C^* = \frac{P_c A_t}{\dot{m}}$, we get:

$$A_t = \frac{\dot{m}}{\frac{P_c}{\sqrt{T_c}} \cdot \sqrt{\frac{\gamma}{R} * \left(\frac{2}{\gamma+1}\right)^{\frac{\gamma+1}{\gamma-1}}}} \tag{3}$$

where $\dot{m} = \frac{F}{v_e}$.

[1] Kerosene has a slightly lower density than water (0.8 g/mL) and LOx a slightly higher one (1.15 g/mL). Treating the rocket as a cylinder is not an accurate model, but one that makes rough calculations easy

2.2.1 Nozzle

The combustion chamber is followed by a conical convergent section and a conical divergent section. The nozzle area expansion ratio was selected to be 3, based on CEARUN data.

2.2.2 Engine Parameters

Propellants	Jet-A/LOx
Chamber Pressure	20.7 bar (300 psi)
Thrust	5 kN (1100 lbf)
Mass Flow Rate	1.96 kg/s (4.33 lbm/s)
O/F Ratio	2.25
C^* (ideal)	1788 m/s (5868 ft/s)
L^*	0.9 m (2.95 ft)
T_c	3400 K
v_e	2550 m/s (8370 ft/s)

2.3 Injector

We chose to use a single element pintle injector for this engine. The working principle of a pintle injector is the impingement of a set of radial jets intersecting perpendicularly with an annular sheet. This creates a conical injection pattern that occurs away from the injector face.

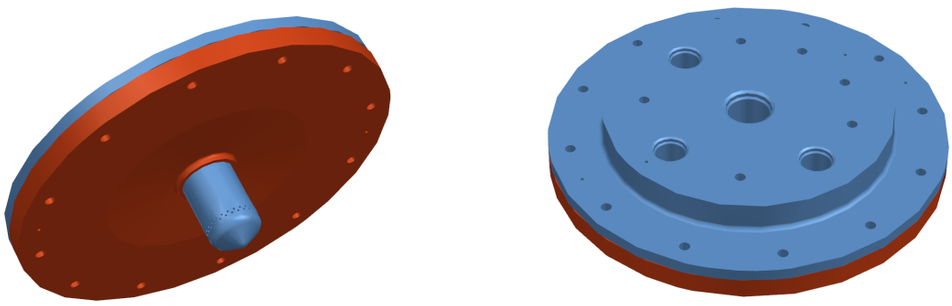

Figure 1: Our injector

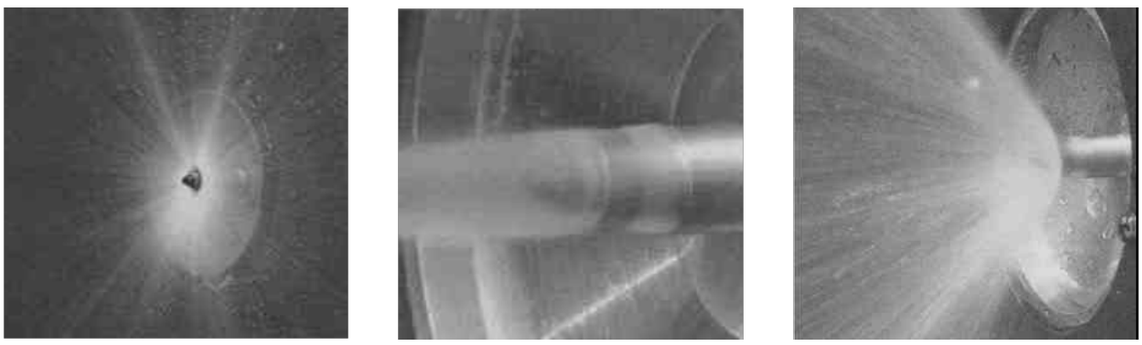

(a) Radial Flow (b) Annular Flow (c) Combined Flows

Figure 2: The pintle injector functions by the impingement of radial jets with an annular tube of liquid [6]

We chose this design for a number of reasons:

1. **Simplicity**

   Since the injector design is radially symmetric, most of it can be made on a lathe, reducing the cost and design complexity. All of the holes that need to be drilled can be drilled normal to the face, reducing the likelihood of damaging drill bits. Additionally, the injector design is modular, so if we damage or detect a manufacturer's defect in one of the pieces, it can be somewhat easily removed and replaced.

2. **Availability of Documentation**

   Knowing little about injector design before starting this project, we were warned against using a like or unlike impingement type injector by students at Purdue, due to there being less available documentation then there is for pintle injectors.

3. **Zucrow Labs Experience**

   Zucrow Labs has tested a number of pintle injectors on their 10k stand, including PSP's Boomie Zoomie injector, which is similar to our own. Consequently, Zucrow Labs staff will have a better understanding of our engine if we use a pintle design versus another injector geometry.

4. **Combustion Stability**

   Pintle injectors create two recirculation zones: an annular-propellant-rich one near the injector face, and a radial-propellant-rich one in the center of the combustion chamber (see Figure 3). The high relative wind created by these recirculation zones dampens acoustic oscillations in the chamber. Additionally the mixing that the recirculation zones provide decreases the amount of combustion that occurs at pressure antinodes in the chamber.

2.3.1 Injector Parameters

Material	304 Stainless Steel
Annular Gap Size, G	0.27 ± 0.05 mm $(0.0106 \pm 0.002$ $in)$
Orifice Diameter, $d_{orifice}$	1.3 mm $(0.051$ $in)$
Axial Discharge Area, A_{axial}	24.88 mm^2 $(0.039$ $in^2)$
Radial Discharge Area, A_{radial}	59.53 mm^2 $(0.092$ $in^2)$
Pintle Diameter, d_p	32.5 mm $(1.28$ $in)$
Skip Distance [12]	0.9
Blockage Factor [4]	0.64
ΔP_f	5.17 bar $(75$ $psi)$
ΔP_o	3.10 bar $(45$ $psi)$
Spray Angle	$73.33° \pm 3.33°$

2.3.2 Annular Gap, Pintle Orifices, and Spray Angle

In order to ensure that the cooler, fuel-rich recirculation zone would be against our injector face, we decided to make LOx our radial propellant and fuel our annular propellant. This decision also allows us to use a standard elastomer o-ring seal on our manifold instead of a PTFE seal, since the propellant in the manifold (Jet-A) will not be at cryogenic temperatures.

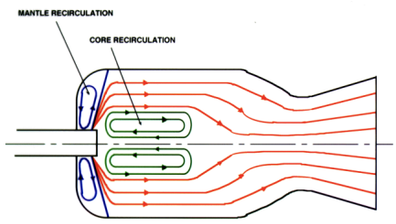

Figure 3: The unique pintle injection geometry creates two recirculation zones in the combustion chamber [6]

Sizing our annular gap, the small, donut-shaped orifice through which our fuel will pass, was one of the most difficult aspects our design process. The primary tradeoff to consider is that between the injector pressure drop and the characteristic spray cone angle of the engine. A low pressure drop would reduce the load on the feed system, as less force is needed to drive the fuel through the annular gap, but it would also reduce the fuel injection velocity. The lower the fuel injection velocity, the greater the spray cone angle of the injector. With a greater spray cone angle, the combustion will occur closer to the injector face, and the spray will impinge with a greater angle of incidence on the combustion chamber walls (see Figure 5). This will increase the thermal load on both the injector and the combustion chamber wall.

Figure 4: The annular gap is the orifice formed by the pintle outer diameter and the injector face

The spray cone angle is driven by a parameter known as the local momentum ratio (LMR), which describes the momentum ratio of a single oxidizer jet to a corresponding section of the annular fuel jet. [9]

$$LMR = \frac{\rho_o U_o^2 A_{radial}}{\rho_f U_f^2 A_{axial}} = \frac{\rho_o U_o^2 * \pi d_{orifice}^2/4}{\rho_f U_f^2 d_{orifice} * G} \tag{4}$$

The pressure drop across the annular gap and pintle drives the sizing of the annular gap and the pintle orifices. The flow area of each propellant injection element (orifices and annular cap) can be determined with the discharge equation:

$$A = \frac{\dot{m}}{C_d \sqrt{2\rho\Delta P}} \tag{5}$$

In order to minimize LMR, and thereby minimize the spray angle, the fuel injection velocity should be maximized, while the oxidizer injection velocity should be minimized. This will "push" the spray cone farther into the combustion chamber. Since velocity is correlated with pressure drop, this means that the pressure drop across the annular gap should be as high as possible, while the pressure drop across the pintle orifices should be as low as possible. In order to keep tank pressure low in future designs, we decided to cap the

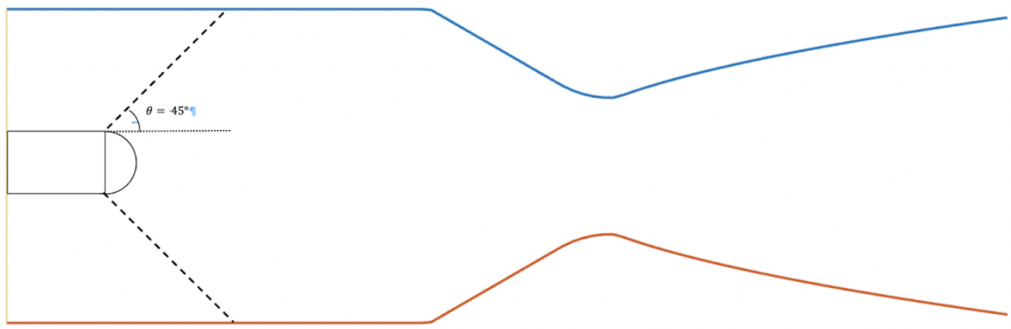

Figure 5: A visualization of the spray cone angle in a combustion chamber

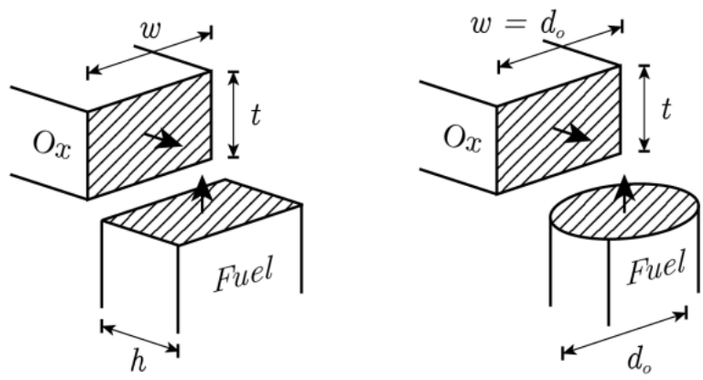

Figure 6: LMR is calculated by determining the momentum of a radial jet (in this diagram, fuel) compared with that of a corresponding section of fluid in the annular stream [9]

pressure drop across the annular gap at 25% of chamber pressure. For the pintle orifices, we decided to set the pressure drop to 15% of chamber pressure; going any lower would run the risk of creating a negative pressure drop across the pintle, allowing for combustion to propagate into the injector, destroying the engine. With these pressure drops set, we can now calculate the total discharge area for both the fuel and the oxidizer. For the axial (fuel) discharge area, we get 24.88 mm^2 (0.039 in^2), and for the radial (oxidizer) discharge area, we get 59.53 mm^2 (0.092 in^2).

We chose the diameter of each orifice to be 1.3 mm (0.0512 in), meaning that the area of each orifice is 1.33 mm^2 (0.0523 in^2). Dividing the total axial discharge area by the area of each orifice, then rounding down, gives us 44 total orifices, or 22 orifices in each row (rounding results in a 1.9% deviation from the theoretical radial discharge area). This results in our design having a blockage factor of 0.64, which is within the recommended range provided by [9]. To calculate the annular gap size, G, we can rearrange the formula that geometrically describes A_{axial}:

$$A_{axial} = \pi((\frac{d_p}{2} + G)^2) - (\frac{d_p}{2})^2) \tag{6}$$

where d_p is the diameter of the pintle. Rearranging, we get

$$G = \sqrt{\frac{A_{axial}}{\pi} + (\frac{d_p}{2})^2} - \frac{d_p}{2} \tag{7}$$

With these parameters set, we can calculate the LMR, then using the empirical correlation outlined in [9], we can calculate the spray angle.

$$\theta = \alpha \arctan(\beta \times LMR) \times \frac{180^\circ}{\pi} + 20^\circ \tag{8}$$

where α and β are defined by the model in [9]. Plugging in 2.00 kg/s (4.41 lbm/s) for our mass flow rate and 2.2 for our O/F ratio, 6.89 bar (100 psi) for our annular gap pressure drop and 4.14 bar (60 psi) for our pintle pressure drop, and taking into account a $\pm 0.05mm$ ($\pm 0.002in$)anufacturing tolerance for G, we find that $\theta \approx 73.33^\circ \pm 3.33^\circ$.

Note: the discharge area equation is a low-quality model due to its high dependence on C_d, a value which can only be determined based on empirical data and is a function of several difficult-to-measure parameters, such as the geometry of the flow field in our injector. Nevertheless, this is the only model we have available to determine our injection element sizes based on pressure drop. Since C_d is so difficult to determine, we have assumed it to be 0.9 for the pintle orifices [2], leading to a small orifice size that we can then make bigger, if needed, after experimentally determining our value for C_d during our water flow test.

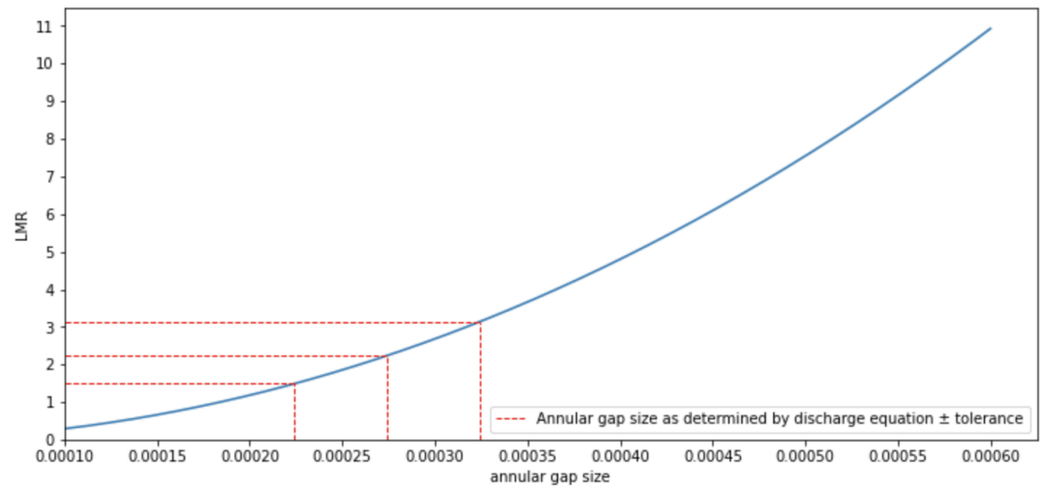

Figure 7: LMR as a function of G

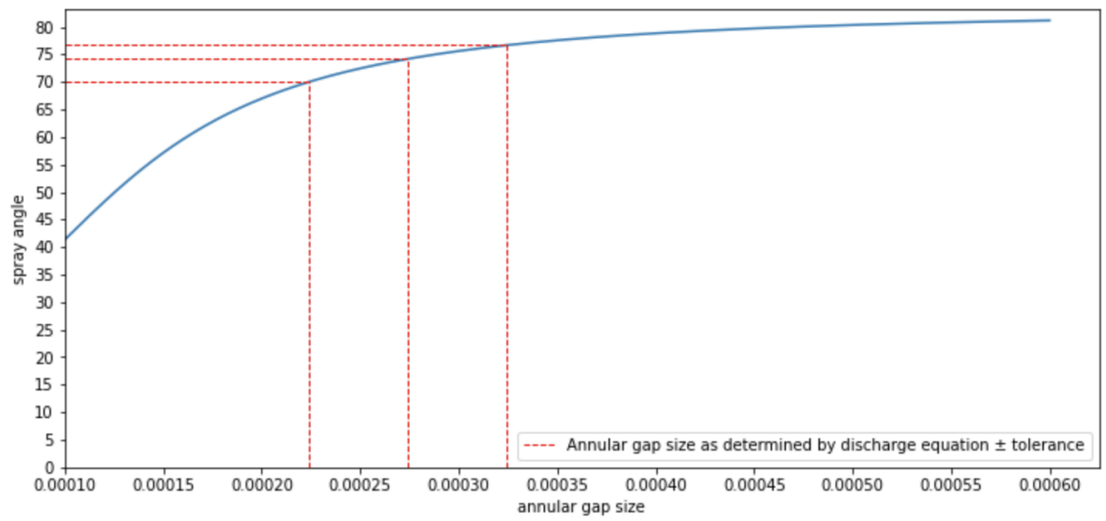

Figure 8: Spray angle as a function of G

2.3.3 Manifold

The injector manifold is shaped to maximize the flow uniformity through the annular gap. The fluid is introduced into the manifold via two ports that are 180 degrees offset from one another. To smooth out startup transients, the manifold slopes slightly upward so that it the propellant must fill it before entering the annular gap.

2.3.4 Manufacturing Technique

The manifold plate (top plate) of our injector will be milled in a CNC lathe, since it is azimuthally symmetric. Once this process is complete, the pintle orifices, fitting ports, and dowel pin sockets will be drilled and the fitting ports will be threaded. A horizontal datum, in the form of two dowel pin sockets, will be milled into the top of the manifold plate so that we have the ability to widen the pintle orifice holes if needed.

2.3.5 Fittings

Both the fuel and oxidizer lines will be connected with F50X fittings, 8-F50X for the fuel and 16-F50X for the oxidizer, rated to 6000 psi. The oxidizer fitting will be milled out to provide a smooth transition from the feed line diameter to the pintle diameter. These fittings were chosen to provide a high-quality seal between the feed lines and manifolds, and because they were recommended to us by our mentors at Zucrow Labs.

2.4 Combustion Chamber

The combustion chamber will be a simple, 4140 steel billet into which we mill a nozzle geometry. The size of the combustion chamber was determined based on burn time, heat transfer into the walls, and manufacturing cost.

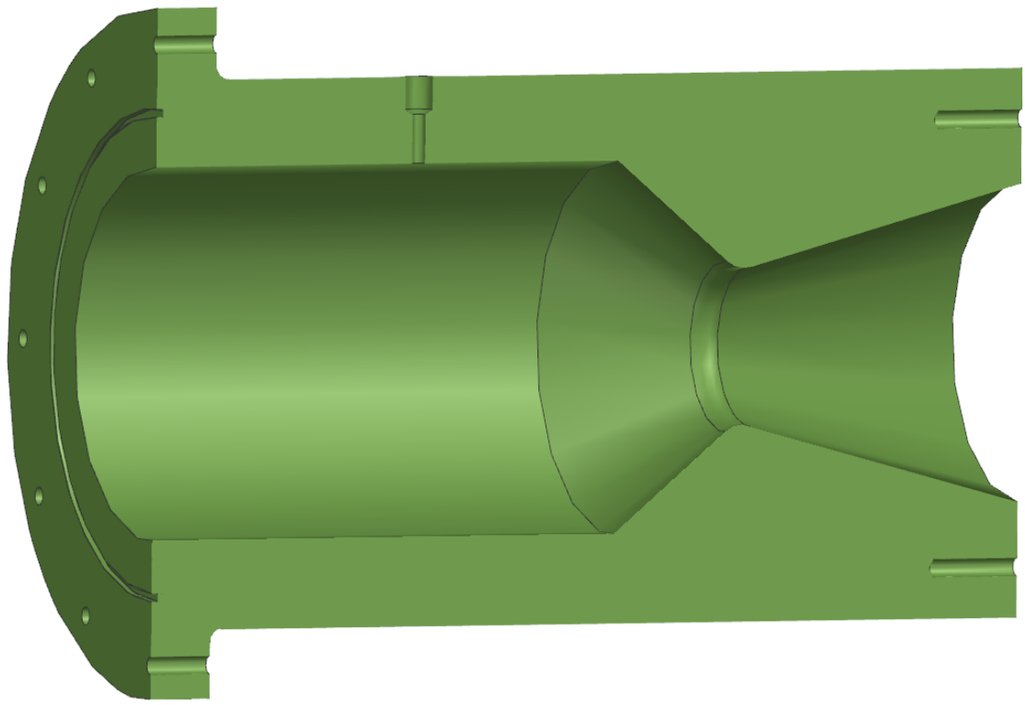

Figure 9: Our combustion chamber

2.4.1 Combustion Chamber Parameters

Volume, V_c	2100 cm^3 (130 in^3)
Length (Nozzle + Chamber)	330 mm (13 in)
Diameter	65 mm (2.56 in)
Wall thickness	30 mm (1.18 in)
Material	4140 Steel

2.4.2 Wall Sizing

Given that our combustion chamber will have no cooling, it is important that it is thick enough to contain the combustion gases for the entirety of the burn duration. To determine the necessary thickness of the combustion chamber, a transient heat transfer calculation was performed.

In the calculation, the combustion chamber was treated as an semi-infinite conducting plate with a convective boundary condition. This is a reasonable approximation since for the burn durations we are targeting, there will be no conduction to the other side of the combustion chamber wall during the burn.

As specified in [10], the equation for heat transfer into a semi-infinite plate is

$$\Theta = \operatorname{erf}\left(\frac{\zeta}{2}\right) + \exp\left(\beta\zeta + \beta^2\right)\operatorname{erfc}\left(\frac{\zeta}{2} + \beta\right) \tag{9}$$

where $\Theta = \frac{T-T_c}{T_i-T_c}$, $\beta = \frac{h\sqrt{a_w t}}{k_w}$, and $\zeta = \frac{x}{\sqrt{a_w t}}$ are dimensionless constants where $T_i = 300K$ is the initial temperature of the chamber wall.

Determining the Heat Transfer Coefficient (h):
To determine the heat transfer coefficient in the combustion chamber, we used the Bartz Correlation as specified in [1]:

$$h = \frac{0.0026}{d_t^{0.2}}\left(\frac{\mu^{0.2}C_p}{Pr^{0.6}}\right)\left(\frac{P_c}{C^*}\right)^{0.8}\left(\frac{d_t}{r_c}\right)^{0.1}\left(\frac{A_t}{A}\right)^{0.9}\sigma \tag{10}$$

A is the cross sectional area of the combustion chamber at the point in question. Pr, μ, and σ can be determined using the empirical correlations provided in [1]. Since h is greatest at the throat, we can make the conservative assumption $\frac{A_t}{A} = 1$ at all points in the combustion chamber. Additionally, $d_t = r_c$ in our design, allowing for further simplification. Plugging in the rest of the parameters for our combustion into (10), we get $h = 19750\frac{W}{m^2K}$. Combining this result with the thermal diffusivity for 4140 steel, we can solve for $T(x,t)$, the temperature profile across the wall using equation (9) and the definition of Θ. Below is a plot showing the time evolution of the temperature profile:

As can be seen in the figure, for burn durations below 0.4 s, there will be no temperature change in the wall at the position of the combustion chamber o-ring during the burn. Furthermore, since there is no

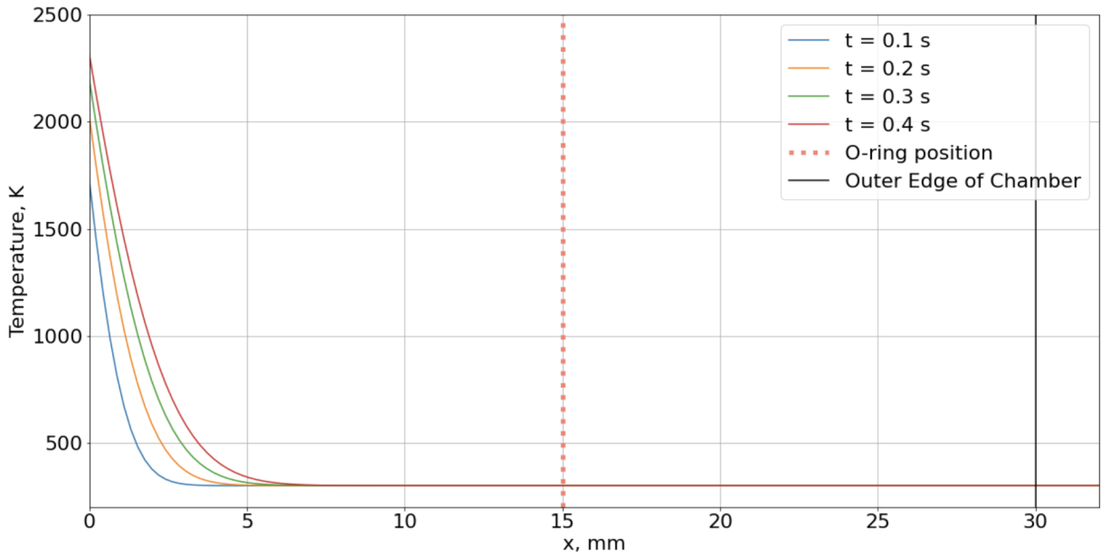

Figure 10: Temperature profile at increasing times t

temperature change on the edge of the chamber, the treatment of the combustion chamber as a semi-infinite plate is valid.

A concern with this model is that it does not take into account the ablation of the combustion chamber wall. As the wall ablates away, new material will be exposed. Given the low thermal diffusivity of the wall material, this effect will likely be more substantial than conduction, hence a conservative burn duration and sizing of the design is prudent.

2.4.3 Seal

The combustion chamber seal will be an AS568-159 PTFE O-ring. PTFE was chosen as the material for our combustion chamber seal since it can withstand higher temperatures than other polymer-based O-rings. This comes at the cost of elasticity, meaning that a new O-ring will be required every time the combustion chamber is attached to the injector.

2.4.4 Bolts

Hooke's Law was used to calculate the required bolt preload for this configuration. A free body diagram of the connection, shown in figure 11, informed the specification of our model. The model does not take into account the forces exerted by the manifold plate on the head plate because it calculates the minimum required preload to keep the assembly together during operation. This assumes that $P_c A_{eff} \leq P_m A_{eff}$, and that the tension provided by the bolt exactly matches the force exerted by the combustion chamber and manifold pressures. The bolts are sized to with a safety factor of 1.5 on the total preload, with the additional tension force being balanced by a compressive force between the manifold and head plate. The model yields the equations:

$$F_{bolts} - P_c A_{eff} - K - O_c = 0 \tag{11}$$

for the combustion chamber plate and

$$K + P_c A_{eff} - P_m A_{eff} + O_c - O_m = 0 \tag{12}$$

for the manifold plate. Solving (11) for K, then substituting into (12), we get:

$$F_{bolts} = P_m A_{eff} + O_m \tag{13}$$

Substituting in 34.5 bar (500 psi) for P_m and $\pi \times (68.2879mm)^2 = 0.0146m^2 = 22.69in^2$ for A_{eff}, then multiplying by the 1.5 safety factor gives us a total clamping force of 6650 N (1495 lbf). To connect the joint, we decided to use 12 SAE Grade 8 1/4-28 bolts, spaced evenly around the flange circumference.

In order to prevent any vibration-induced loosening (an unlikely event, given our burn duration), we will use distorted thread locknuts to increase the friction between the nuts and the bolt shafts. Elliptical locknuts were chosen for their simplicity, tolerance of high temperatures, and ease of disassembly.

2.5 Ignition System

The engine will be ignited with a piece of solid propellant placed in the combustion chamber near the injector. We chose this method of ignition over a hydrogen torch igniter because we want to gain experience with the ignition technology that we would be using in the field, where access to a hydrogen torch would be difficult. We will include more information about our ignition system design in our Test Readiness Review.

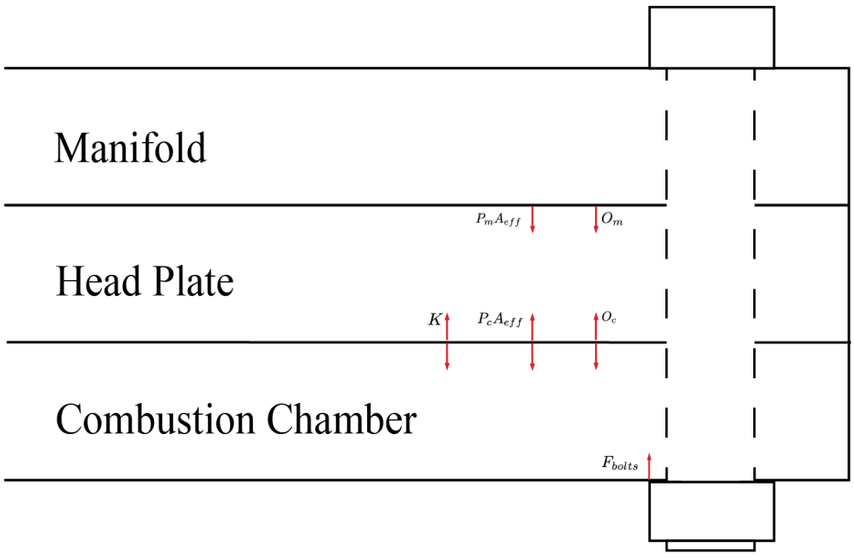

Figure 11: Free body diagram of the bolt connection with minimum bolt tension

3 Risks

Given our short burn duration, the risks associated with our test campaign are greatly reduced, but not eliminated. There are still several ways our engine could undergo a "rapid unscheduled disassembly."

3.1 Hard Start

The most likely failure mode for our engine is a hard start: a pressure spike that can occur shortly after ignition as a result of one of the following causes.

1. **Inadequate igniter placement**
   If the igniter is not placed near the injector, unburnt propellant can build up in the combustion chamber before it reaches the igniter, causing an explosion that can damage the test infrastructure. We will mitigate this risk by placing the igniter just below the pintle tip.

2. **Premature introduction of propellant**
   If there is not an ignition source present in the engine at the time of propellant introduction, this will lead to a buildup of unburnt propellant in the engine, causing an explosion at the time of ignition. We will mitigate this risk by testing the ignition system prior to the hot fire test, as well as measuring the propellant introduction times during the cold flow test.

3.2 Injector Burnthrough

Due to the high temperatures present in the combustion chamber, there is a chance that the injector will burn through. According to the semi-infinite plate model used in Section 2.4.2, thermal effects, assuming a high heat transfer coefficient, will only be present to a distance of roughly 5 mm (0.2 in) for a 0.4 s burn duration.

3.3 Seal Burnthrough

The melting point of our PTFE seal is roughly 330 °C, while our adiabatic flame temperature is roughly 3100 °C. There are a few measures we are taking to mitigate this risk. The first is to offset the o-ring inner diameter from the combustion chamber by 15 mm. This will create a small thermal standoff, lowering the temperatures to which the o-ring is exposed. Additionally, our low burn time will prevent the o-ring from reaching an equilibrium temperature, keeping it from overheating.

3.4 Inadequate Seal

PTFE is an inelastic material, meaning that it will not return to its original form factor after it has been compressed. If installed incorrectly, this compression set could cause there to be a gap between the seal and the groove, leading to high pressure and high temperature combustion gases spewing out past the seal, creating a jet.

Additionally, PTFE is a harder material than most elastomers, meaning that it does not conform as well to surfaces compared to other o-ring materials. If the finish on our groove is not fine enough, surface irregularities could lead to a gap between our o-ring and our groove, causing combustion gases to jet out of the connection.

We will mitigate this risk by performing a static pressure test on our engine before we fire it. This will verify the seal integrity for all of the seals in our design.

4 Instrumentation

4.1 Combustion Chamber Pressure Transducer

The pressure transducer will be mounted onto the combustion chamber, with a 6" long standoff line to reduce the thermal load on it. Additionally, the pressure transducer fitting port will be a blind hole with a small orifice drilled in the end to further reduce the thermal load on the fitting.

4.2 Manifold Pressure Transducer

A second pressure transducer will be located in the manifold. The purpose of this pressure transducer will be to measure head loss due to our interface plumbing, and to verify our injector pressure drop during the hot fire.

5 Testing

Below is an outline of our test matrix. More detailed testing procedures will be created for our Test Readiness Review.

Test	**Objectives**
Fit Check	Check that the engine can be assembled, verify O-ring groove depth
Water Flow	Check C_d, flow uniformity, and that orifices are not blocked
Static Pressure Test	Verify combustion chamber and manifold seals and bolt integrity
Ignition Test	Verify performance of solid propellant ignition system
Cold Flow	Measure propellant introduction times and verify interface with Zucrow Labs feed system
Hot Fire	Verify primary and secondary requirements

6 Conclusion

The main design considerations for our 5 kN Grunt engine have been outlined, including project goals, functionality, and failure modes. If no major flaws in our design are uncovered, our next steps will be to manufacture the engine and perform the water flow test on our design.

7 Acknowledgements

We would like to acknowledge those who have helped us prepare this design for testing. Thomas White, our mentor, has provided invaluable technical advice and accountability, helping us narrow down our objectives by asking the tough questions. We extend our gratitude to David Williams, our machinist, for taking so much time to answer basic questions about manufacturing. Chris Nilsen, our liaison at Purdue, has also been incredibly helpful, providing us with information about Zucrow Labs' test stand and procedures, as well as feedback on our design. Scott Meyer, the managing director at Zucrow Labs, has also provided us with a ton of help with our interface design, fitting sizing, and logistics as we begin to work more closely with Purdue. We would also like to thank the Purdue Space Program student organization, specifically Benjamin Worrell, for reviewing our preliminary design review, providing feedback, and helping us get started on our design. Additionally, we would like to give credit to Nate Campbell, the propulsion director at MASA, for consulting with us about our combustion chamber.

This project would not be possible without support from the Purdue Department of Aerospace Engineering and Maurice J. Zucrow Laboratories, the University of Illinois AIAA Chapter, and funding from the Illinois Space Grant Consortium. Thank you for your support!

References

[1] D. R. Bartz. "A Simple Equation for Rapid Estimation of Rocket Nozzle Convective Heat Transfer Coefficients". In: *Journal of Jet Propulsion* (1957). DOI: https://doi.org/10.2514/8.12572.

[2] G.S. Gill and W.H. Nurick. *Liquid Rocket Engine Injectors*. National Aeronautics and Space Administration, 1976, p. 38.

[3] Bonnie J. Mcbride and Sanford Gordon. "Computer Program for Calculation of Complex Chemical Equilibrium Compositions and Applications II. Users Manual and Program Description". In: (1996).

[4] Stephen D. Heister. "Pintle Injectors". In: *Handbook of Atomization and Sprays*. Ed. by Nasser Ashgriz. Springer Science + Business Media, LLC, 2011. Chap. 18, pp. 647–656.

[5] Robert A. Brauenig. *Basics of Space Flight: Rocket Propulsion*. 2012. URL: http://www.braeunig.us/space/propuls.htm (visited on 02/26/2022).

[6] Gordon A. Dressler and J. Martin Bauer. "TRW Pintle Engine Heritage and Performance Characteristics". In: *Aerospace Research Central* (2012). DOI: http://dx.doi.org/10.2514/6.2000-3871.

[7] Utah State University. *Section 5, Lecture 1: Review of Idealized Nozzle Theory*. 2016. URL: http://mae-nas.eng.usu.edu/MAE_5540_Web/propulsion_systems/section5/Section_5.2.pdf (visited on 02/14/2022).

[8] Isang Yu et al. "Combustion Performance of a Pintle Injector Rocket Engine with Canted Slit Shape by Characteristic Length and Total Momentum Ratio". In: *Journal of the Korean Society of Propulsion Engineers* (2017). DOI: http://dx.doi.org/10.6108/KSPE.2017.21.1.036.

[9] James Blakely, Johann Freeberg, and Jacob Hogge. "Spray Cone Formation from Pintle-Type Injector Systems in Liquid Rocket Engines". In: *AIAA SciTech Forum* (2019). DOI: https://doi.org/10.2514/6.2019-0152.

[10] John H. Lienhard IV and John H Lienhard V. *A Heat Transfer Textbook*. Cambridge, MA: Phlogiston Press, 2019. Chap. 5.

[11] Taj Wali Khan and Ihtzaz Qamar. "Factors Affecting Characteristic Length of the Combustion Chamber of Liquid Propellant Rocket Engines". In: *Mehran University Research Journal of Engineering and Technology* (2019). DOI: http://dx.doi.org/10.22581/muet1982.1903.16.

[12] Suji Lee, Jaye Koo, and Youngbin Yoon. "Effects of skip distance on the spray characteristics of a pintle injector". In: *Acta Astronautica* (2020). DOI: https://doi.org/10.1016/j.actaastro.2020.09.043.

A Thrust Chamber Script

```
%% THRUST CHAMBER SIZING PROCEDURE

% Aim: defining thrust chamber geometry from F, O/F ratio, p_0, r_cc

% Intervention needed in STEP 1 (CEA) and in STEP 3 (Getting angles from
% table in chapter 8 notes)

format long; clear all; close all; clc;

%% CONSTANTS
P_a       = 101325;       % Pa

%% INPUT
F         = 5000;         % N
OF_ratio  = 2.25;
p_0       = 20e+5;       % Pa
p_e       = P_a;
R_c       = 0.06;         % m (comb. chamb. radius)


% STATES
% 0  Combustion chamber after combustion
% T  Throat
% E  Exit

%% STEP 1: CEA (MASS FLOW INDEPENDENT)

% Go to https://cearun.grc.nasa.gov and run a simulation with the data
% above.
%
% With the following input:
% P_0                                          400 psia
% o/f                                          2.25
% Exit conditions: P_c/P_e                     27.239082161361953
% Consider Ionized Species as possible products? Yes
```

```
%
% we get the following results:

T_0    = 3440.69;      % K
gamma  = 1.1976;       %                    (exit)
Cp     = 2.3183e3;     % J/(kg)(K)          (exit)

v_e    = 2646.9;       % m/s                (exit isp)
M_e    = 2.661;
eps    = 4.7409;       % expansion ratio (exit Ae/A_t)

%% STEP 2: MASS FLOW DEPENDENT CALCULATIONS

% First get R
Cv = Cp/gamma;
R = Cp-Cv;                % Specific gas constant

% We can calculate the needed mass flow for the required thrust
m_dot = F/v_e;

% That conditions throat area, and we can obtain it from the chocked flow
% mass flow rate equation.
% m_dot = p_0*A_t/sqrt(T_0)*sqrt(gamma/R*(2/(gamma+1))^((gamma+1)/(gamma-1)));

A_t =m_dot/(p_0/sqrt(T_0)*sqrt(gamma/R*(2/(gamma+1))^((gamma+1)/(gamma-1))));

% The compression ratio will be
eps_c = (pi*R_c^2)/A_t;

% Combustion chamber sizing
% Needed combustion chamber volume can be calculated in the following way
% V_chamber = L_characteristic * A_throat
% For LOX/RP1 the characteristic length is 76-102 cm. Lets pick 90cm.
L_characteristic = 1;              % m (for RP1-LOX should be 0.9m, but...
                                   %   being conservative, let's go with 1.)
V_chamber = L_characteristic*A_t; % m^3

% If we want the combustion chamber radius to be r_cc, then we need a
% length:
L_c = V_chamber/(pi*R_c^2);

%% STEP 3: GEOMETRICAL PARAMETERS FOR THE NOZZLE

R_t = sqrt(A_t/pi);
R_e = sqrt(eps)*R_t;

% Arbitrary
Theta_c = 30;     % deg
% FROM THE TABLE IN CHAPTER 8 NOTES
Theta_n = 20;     % deg
Theta_e = 8;      % deg

%% STEP 4: Solving geometry

syms x A1 A2 B1 B2 C1 C2 D1 D2 D3 xa xab xcd xd;
ya     = A1*x + A2;
dya_dx = diff(ya,x);
yb     = -sqrt((1.5*R_t)^2-(x-B1)^2) + B2;
dyb_dx = diff(yb,x);
yc     = -sqrt((0.382*R_t)^2-(x-C1)^2) + C2;
dyc_dx = diff(yc,x);
yd     = sqrt(D1*x-D2)+D3;
dyd_dx = diff(yd,x);

% Solving throat
S = solve([subs(yb, x, 0)      == R_t,...
           subs(yc, x, 0)      == R_t,...
           subs(dyb_dx, x, 0)  == 0,...
           subs(dyc_dx, x, 0)  == 0],...
           [B1 B2 C1 C2]);
yb     = subs(yb,[B1,B2],[S.B1,S.B2]);
dyb_dx = diff(yb,x);
```

```
yc      = subs(yc,[C1,C2],[S.C1,S.C2]);
dyc_dx = diff(yc,x);

% Solving throat circunferences' limits
S = vpasolve([subs(dyb_dx, x, xab)  == -tand(Theta_c),...
              subs(dyc_dx, x, xcd)  == tand(Theta_n)],...
              [xab xcd]);
clear xab xcd
xab = S.xab; xcd = S.xcd;
clear S

% Solving diverging section

S = solve([subs(dyd_dx, x, xcd) == tand(Theta_n),...
              subs(dyd_dx, x, xd)  == tand(Theta_e), ...
              subs(yd, x, xcd)  == subs(yc,x, xcd),...
              subs(yd, x, xd)  == R_e],...
              [D1 D2 D3 xd]);

yd      = subs(yd,[D1,D2,D3],[S.D1,S.D2,S.D3]);
dyd_dx = diff(yd,x);

clear xd
xd = S.xd;
clear S

% Solving converging section
S = solve([subs(dya_dx, x, xab) == -tand(Theta_c),...
              subs(ya, x, xab)  == subs(yb,x, xab),...
              subs(ya, x, xa)  == R_c],...
              [A1 A2 xa]);

ya      = subs(ya,[A1,A2,xa],[S.A1,S.A2,S.xa]);
dya_dx = diff(ya,x);

clear xa
xa = S.xa;
clear S


%% OUTPUT

xcc = xa-L_c;
xx=linspace(xa-L_c,xd);
nn=nozzle(xx,ya,yb,yc,yd,xa,xab,xcd,xd,L_c,R_c);
plot([fliplr(xx),xx], [fliplr(-nn), nn], 'linewidth', 2)
hold on;
xlabel('[m]')
ylabel('[m]')


axis equal
ax=gca;
xlim (1.2*ax.XLim)
ylim([-1.2*max([R_c,R_e]),1.2*max([R_c,R_e])])


%% FUNCTION DECLARATION

function yy = nozzle(xx,ya,yb,yc,yd,xa,xab,xcd,xd,L_c,R_c)
    yy=zeros(size(xx));
    for i = 1:length(xx)
        if xx(i)>=xa-L_c && xx(i)<xa
            yy(i) = R_c;
        elseif xx(i)>=xa && xx(i)<xab
            yy(i) = subs(ya,xx(i));
        elseif xx(i)>=xab && xx(i)<0
            yy(i) = subs(yb,xx(i));
        elseif xx(i)>=0 && xx(i)<xcd
            yy(i) = subs(yc,xx(i));
        elseif xx(i)>=xcd && xx(i)<=xd
            yy(i) = subs(yd,xx(i));
```

```
            end
        end
    end
```